arXiv:2510.11303v2 [cs.CV] 13 May 2026

SKETCH2SYMM: SYMMETRY-AWARE SKETCH-TO-SHAPE GENERATION VIA SEMANTIC BRIDGING

Yan Zhou[1], *Mingji Li*[2*], *Xiantao Zeng*[2], *Jie Lin*[1], *Yuexia Zhou*[1]

[1]School of Electronic Information Engineering, Foshan University, Guangdong, China
[2]School of Computer Science and Artificial Intelligence, Foshan University, Guangdong, China

ABSTRACT

Sketch-based 3D reconstruction remains a challenging task due to the abstract and sparse nature of sketch inputs, which often lack sufficient semantic and geometric information. To address this, we propose Sketch2Symm, a two-stage generation method that produces geometrically consistent 3D shapes from sketches. Our approach introduces semantic bridging via sketch-to-image translation to enrich sparse sketch representations, and incorporates symmetry constraints as geometric priors to leverage the structural regularity commonly found in everyday objects. Experiments on mainstream sketch datasets demonstrate that our method achieves superior performance compared to existing sketch-based reconstruction methods in terms of Chamfer Distance, Earth Mover's Distance, and F-Score, verifying the effectiveness of the proposed semantic bridging and symmetry-aware design.

***Index Terms*—** Sketch-to-image translation, 3D shape reconstruction, symmetry loss

1. INTRODUCTION

In recent years, the rapid advancement of deep learning has significantly accelerated progress in 3D shape reconstruction from 2D images, opening up broad application prospects. Accurately generating 3D shapes from 2D images enhances realism and precision, which is crucial for industries such as virtual reality, robotics, and manufacturing. Effectively leveraging the rich visual information contained in 2D images to reconstruct 3D shapes is key to improving the efficiency and quality of digital representations. However, in real-world scenarios, sketches are often a more common and accessible form of expression. Therefore, extending the research focus from image-driven to sketch-driven 3D reconstruction holds substantial importance.

Compared with images that contain rich visual cues such as color, texture, and shading, sketches inherently suffer from sparsity and abstraction. To address these challenges, existing studies have explored various strategies, including style normalization [15], data augmentation [16], and additional priors such as viewpoint estimation [17, 18] and multi-view sketches [19, 20, 21]. Some approaches also leverage learned 3D shape priors [22]. Representative works include: SketchSampler [16], which translates sketches into more informative 2D representations via image-to-image networks; PASTA [26], which integrates sketches with text descriptions in vision–language models; S3D [27], which introduces style alignment loss and augmentation; and SketchDream [28], which employs a sketch-based multi-view image diffusion model with depth guidance. Additionally, image translation has advanced rapidly, with CoCosNet [35] emerging as a powerful and extensible framework that has inspired numerous task-specific studies. Some works introduce contrastive learning to enhance cross-domain invariant feature modeling [36], while others explore unpaired exemplar-guided translation to improve domain transfer [37]. These advances in image translation have also provided insights and inspiration for sketch-to-shape generation tasks.

Despite extensive exploration, existing methods still show limited generalization to sketches of varying styles and often fail to fully exploit their sparse information. Meanwhile, many everyday objects exhibit strong symmetry [31], which humans frequently rely on in perception and imagination. For example, one can infer the missing half of a chair from only one side. However, current approaches rarely model symmetry explicitly, and the inherent sparsity and abstraction of sketches make it difficult to leverage symmetry effectively. Therefore, translating sketches into images as a semantic bridge becomes crucial for both enriching sparse representations and enabling effective symmetry modeling.

To address this, we propose a sketch-based two-stage 3D reconstruction method. In the first stage, we perform sketch-to-image translation, extending CoCosNet [35] for this specific task. This allows sketches to be effectively transformed into semantically rich images, serving as more informative and structured intermediate representations that bridge the domain gap and improve the accuracy of subsequent 3D prediction. In the second stage, the intermediate images are fed into a geometry-aware network for 3D shape reconstruction. During training, we incorporate an explicit symmetry constraint as a geometric prior, which compensates for the lack of 3D structural cues in sketches and encourages the generation of more complete and regular 3D structures.

The main contributions of this paper can be summarized as: 1) We propose a semantic bridging strategy via sketch-to-image translation, which enriches sketch representations and facilitates more effective 3D reconstruction. 2) A geometric symmetry constraint is incorporated during training as an explicit prior to encourage object-level structural regularity, improving the completeness and plausibility of reconstructed shapes. 3) We perform extensive experiments on public sketch datasets, demonstrating superior performance in reconstruction accuracy, generalization, and robustness compared to representative sketch-based 3D generation methods.

*© 2025 IEEE. Personal use of this material is permitted. Permission from IEEE must be obtained for all other uses, in any current or future media, including reprinting/republishing this material for advertising or promotional purposes, creating new collective works, for resale or redistribution to servers or lists, or reuse of any copyrighted component of this work in other works.

2. METHOD

We propose Sketch2Symm, a two-stage method for sketch-based 3D shape reconstruction. The training procedure of both stages is illustrated in Fig. 1. The first stage (Section 2.1) employs a cross-domain image translation network to convert sparse sketches into semantically enriched images, thereby enhancing the geometric cues available for reconstruction. The second stage (Section 2.2) incorporates a symmetry-based loss into an image-to-point-cloud generation pipeline, encouraging structural regularity and detail preservation. The two stages are trained independently to address the semantic sparsity and structural ambiguity inherent in sketches. During inference (Section 2.3), a single sketch is processed sequentially through both stages to produce a structurally consistent 3D point cloud.

2.1. Stage 1: Sketch-to-Image Translation

The abstractness and sparsity of sketches limit the available semantic information, which poses significant challenges for 3D reconstruction. To mitigate this issue, we first synthesize shape-consistent images from input sketches. This step enriches the sketch representation by leveraging the richer semantic capacity of natural images, thereby compensating for the limited information in sketches.

In the first stage, the processing pipeline begins with multi-scale feature extraction using a pre-trained VGG-19 model [45], which processes both input sketches and reference images to obtain hierarchical feature representations. These features are then fed into the Deformation Alignment Network, as illustrated in Fig. 1(a), which establishes pixel-wise correspondences between cross-domain inputs through deep feature correlation and cosine similarity computation. This cross-modal alignment deforms the geometric structure of the reference image to match the sketch, thereby guiding the image synthesis process in the downstream adversarial network.

In the Deformation Alignment Network, we establish cross-domain deep correspondences between sketch and reference image. We first construct a shared semantic space s within the latent feature domain to align the representations of input sketches and reference images. Specifically, an input sketch x is mapped to its feature representation x_s, while a reference image y is mapped to its feature representation y_s. In the shared space s, we employ cosine similarity as the similarity metric. By maximizing the cosine similarity between x_s and y_s, we encourage the two representations to be directionally consistent and semantically aligned. The cosine similarity is defined as:

$$\cos(\theta) = \frac{x_s^T y_s}{\|x_s\|_2 \cdot \|y_s\|_2}, \tag{1}$$

and our optimization objective is formulated as:

$$\max_{\theta_x, \theta_y} \frac{x_s^T y_s}{\|x_s\|_2 \cdot \|y_s\|_2}, \tag{2}$$

which enforces semantic alignment between sketches and reference images in the shared domain.

Due to the inherent lack of chromatic and textural information in sketch inputs, which requires full reliance on reference images for color and texture synthesis, we introduce the Dual-Attention Color Enhancement (DACE) module to enable adaptive feature refinement, as illustrated in the generator part of Fig. 1(a). DACE is located at the final layer of the generator and employs a collaborative dual-attention mechanism through two dedicated branches. Firstly, to adapt the feature vectors to the input of DACE, we apply a Channel Reduction defined as:

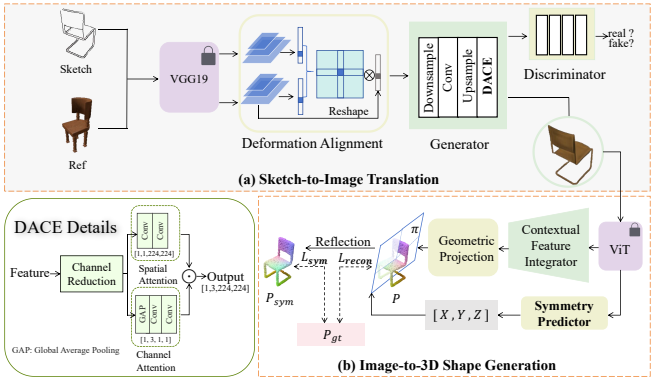

Fig. 1. The two-stage training pipeline of Sketch2Symm. (a) illustrates the training process of Stage 1 from left to right. (b) shows the training process of Stage 2 from right to left. The bottom left corner shows the details of DACE.

$$\max(1, in_channels//factor). \tag{3}$$

We set the factor to 4 with the aim of effectively reducing the computational cost by about 50% while still retaining sufficient representational capacity. The spatial attention branch learns positional importance via two cascaded convolutions, emphasizing geometric regions that require enhanced coloration. The channel attention branch first applies global average pooling, followed by two convolutional layers, to capture inter-channel dependencies and adaptively adjust the enhancement strength of each color component through a channel importance learning mechanism. The optimized attention features from both branches are then fused via element-wise multiplication with broadcasting. This hierarchical attention fusion markedly improves color fidelity and visual realism, while alleviating texture misalignment issues in cross-modal synthesis tasks.

2.2. Stage 2: Image-to-3D Shape Generation

After completing the generation from sketches to images in the first stage, the second stage aims to further reconstruct 3D shapes with geometric consistency. To enhance structural plausibility, we introduce a symmetry constraint during the generation process. We adopt point cloud as the 3D representation, as its coordinate-based form naturally supports the application of symmetry through geometric transformations.

Among existing image-to-3D reconstruction methods, we adopt RGB2Point [30] as the baseline for the second stage, due to its simple encoder-decoder architecture and coordinate-based output. It uses a pre-trained Vision Transformer (ViT) [46] to extract semantic features from the input image, which are then enhanced by a Contextual Feature Integrator and mapped to 3D point coordinates via Geometric Projection. This direct coordinate prediction facilitates the incorporation of explicit geometric constraint. To further improve structural plausibility, we introduce a symmetry constraint during training as an additional regularization term. By defining a reflective mapping in 3D space, each predicted point is paired with its mirrored counterpart, encouraging the model to better capture the inherent symmetry present in many objects.

To explicitly model the symmetrical structures commonly found in real-world objects, we introduce the symmetry constraint during the generation process. Specifically, as illustrated in Fig. 1(b), we assume that there exists a symmetric plane π, which is parameterized

by the unit normal vector $\mathbf{n} = [X, Y, Z] \in \mathbb{R}^3$ and the offset $d \in \mathbb{R}$, and its geometric definition is:

$$\pi : \mathbf{n}^\top \mathbf{x} + d = 0. \tag{4}$$

To predict the symmetry plane from input images, we introduce a Symmetry Predictor module that takes the extracted image features as input and outputs the normal vector components through a Multi-layer Perceptron with ReLU activations. The predicted normal vector is then used to construct a 3×3 reflection matrix $\mathbf{R}$ according to the formula $\mathbf{R} = \mathbf{I} - 2\mathbf{n}\mathbf{n}^\top$, where $\mathbf{I}$ is the identity matrix. For each 3D point $\mathbf{p}_i$ generated by the network, we construct its symmetric counterpart $\mathbf{p}_i^*$ about the symmetry plane using the reflection transformation:

$$\mathbf{p}_i^* = \mathbf{p}_i - 2(\mathbf{n}^\top \mathbf{p}_i + d)\mathbf{n} = \mathbf{R}\mathbf{p}_i. \tag{5}$$

As shown in Fig. 1(b), our network simultaneously generates both the original point cloud P and its symmetric counterpart P_{sym} by applying the reflection matrix to all generated points. The symmetry constraint is enforced through a dual supervision strategy:

$$\mathcal{L}_{3D} = \mathcal{L}_{\text{recon}}(P, P_{\text{gt}}) + \mathcal{L}_{\text{sym}}(P_{\text{sym}}, P_{\text{gt}}), \tag{6}$$

where $\mathcal{L}_{\text{recon}}$ represents the original RGB2Point [30] reconstruction loss, and $\mathcal{L}_{\text{sym}}$ adopts the same reconstruction loss formulation as $\mathcal{L}_{\text{recon}}$ to measure the geometric similarity between the symmetric point cloud and ground-truth. This dual supervision encourages the network to generate point clouds that not only match the ground-truth directly, but also maintain consistency when reflected across the predicted symmetry plane, effectively enforcing geometric symmetry in the generated 3D structures.

2.3. Inference

In the first inference stage, the same frozen VGG-19 model [45] used during training is adopted for feature extraction. Unlike training, no user-provided reference images are required at inference; instead, the system uses fixed reference images. This design is motivated by the use of sketch–reference pairs during training to improve generalization, whereas inference focuses on enriching sketches with image-level color and texture.

In the second stage, a frozen pre-trained ViT [46] extracts features from the synthesized image, which are then fed into the Contextual Feature Integrator and Geometric Projection Module for point cloud reconstruction. Unlike the training phase, symmetric plane prediction is not required during inference. By sequentially executing these two stages, the method produces a complete and structurally consistent point cloud.

3. EXPERIMENTS

3.1. Experimental Settings

3.1.1. Datasets

To support our two-stage training pipeline, we employ the ShapeNet-Synthetic [17] sketch dataset and the image dataset by Xu et al. [32]. Both datasets are derived from the ShapeNet Core dataset [34] with corresponding categories and shapes. For the first training stage, we use the ShapeNet-Synthetic dataset and Xu et al.'s dataset. For the second training stage, we use the rendered images and their corresponding 3D shapes from the ShapeNet Core dataset. For performance evaluation, we utilize both the ShapeNet-Synthetic dataset and the ShapeNet-Sketch [17] dataset, which contains hand-drawn sketches derived from the ShapeNet Core dataset.

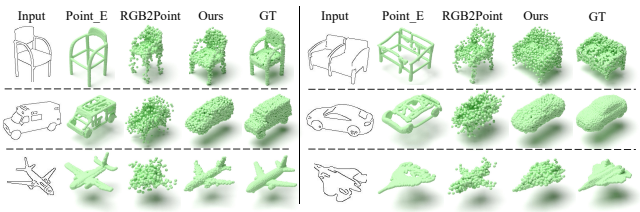

Fig. 2. Visualization of qualitative comparison on the ShapeNet-Synthetic dataset using synthetic sketches.

3.1.2. Evaluation Metrics

To quantitatively evaluate the quality of the generated 3D point clouds, we employ three widely adopted metrics: Chamfer Distance (CD), Earth Mover's Distance (EMD), and F-Score. F-Score is computed with a threshold of 0.01.

3.1.3. Implementation Details

All training and evaluation are conducted on a single 24GB NVIDIA RTX 3090Ti GPU, with the model configured to generate point clouds containing 2048 points. In the training of Stage 1, we use the Adam optimizer with learning rates of 1×10^{-4} for the generator and 4×10^{-4} for the discriminator, applying spectral normalization to ensure training stability. In the training of Stage 2, we use the Adam optimizer with an initial learning rate of 5×10^{-4}, applying learning rate decay with a factor of 0.7 when the validation loss plateaus, and using gradient clipping with a maximum norm of 5.0.

3.2. Quantitative Analysis

In Table 1, our method achieves the lowest CD values across all thirteen object categories in the ShapeNet-Synthetic [17] dataset, demonstrating superior performance compared to existing representative methods. In addition to CD, we further evaluate EMD and F-score in three classic categories: Chair, Car, and Airplane, and compare the results among three representative methods. The results are reported in the upper part of Table 2. Our method achieves the lowest EMD scores across all categories, indicating better performance in point cloud alignment and structural consistency.

3.3. Qualitative Analysis

To qualitatively evaluate reconstruction quality, we focus on three categories: Chair, Car, and Airplane, conducting detailed visual assessments. we visualize the generated point clouds in Fig. 2 and Fig. 3, comparing our method with the representative point cloud reconstruction method Point_E [43] and the baseline RGB2Point [30]. Fig. 2 uses synthetic sketches from the ShapeNet-Synthetic [17] dataset, while Fig. 3 uses hand-drawn sketches from the ShapeNet-Sketch [17] dataset. As demonstrated, our approach demonstrates superior capability in recovering both global structural coherence and fine-grained local details, irrespective of whether the input is a synthetic or hand-drawn sketch.

3.4. Ablation Studies

To validate the effectiveness of our proposed components, we conduct ablation experiments on three categories, focusing on the independent contributions of two core components: the intermediate

Table 1. Quantitative comparison of CD on thirteen categories. CD values are multiplied by 10^3.

Method	Chamfer Distance ↓						
	Car	Sofa	Airplane	Bench	Display	Chair	Table
DISN [32]	7.90	17.65	11.59	12.97	16.63	15.17	25.86
Sketch2Model [17]	15.26	42.35	22.94	23.31	24.07	61.96	21.87
Sketch2Mesh [42]	11.48	25.73	9.29	9.01	15.67	16.83	17.81
Deep3DSketch [41]	12.57	43.96	23.41	23.54	23.31	61.27	20.84
Deep3DSketch-im [40]	7.42	17.76	11.72	13.61	16.90	15.35	25.72
Ours	**2.10**	**4.70**	**1.50**	**5.00**	**5.70**	**5.00**	**7.50**

Method	Chamfer Distance ↓						
	Telephone	Cabinet	Loudspeaker	Watercraft	Lamp	Rifle	Average
DISN [32]	8.79	16.08	18.67	16.24	40.30	8.03	16.53
Sketch2Model [17]	18.82	18.67	20.73	15.72	60.34	19.00	28.08
Sketch2Mesh [42]	17.62	20.44	12.06	8.99	33.29	8.87	15.93
Deep3DSketch [41]	16.11	18.36	22.23	15.25	56.41	19.30	27.43
Deep3DSketch-im [40]	8.66	15.85	19.04	16.18	30.38	7.95	15.89
Ours	**2.60**	**8.50**	**10.80**	**3.40**	**7.90**	**1.70**	**5.11**

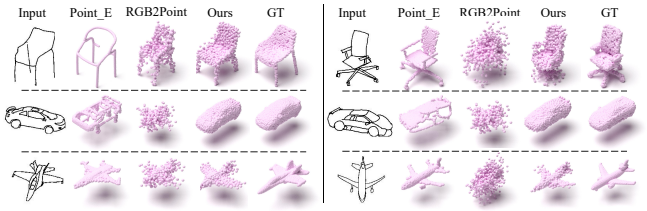

Fig. 3. Visualization of qualitative comparison on the ShapeNet-Sketch dataset using hand-drawn sketches.

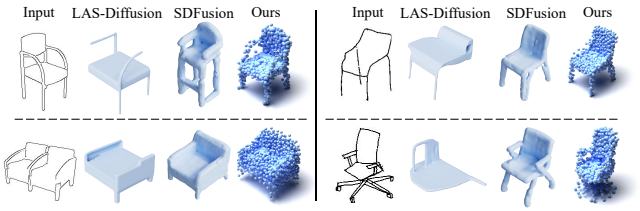

Fig. 4. Qualitative comparison with diffusion-based methods on synthetic and hand-drawn sketches.

sketch-to-image generation step and the symmetry constraint. The first variant removes the sketch-to-image module to assess the impact of semantically enriched images on 3D reconstruction; the second variant excludes the symmetry constraint to evaluate its effect on structural regularity in the generated shapes.

We compare these two ablation variants with our complete method. In the lower of Table 2 reports the results using EMD, and F-Score as evaluation metrics. Removing the sketch-to-image module results in the most significant performance degradation, underscoring its importance. Overall, the complete method achieves the best performance across all metrics, validating the complementary roles of the sketch-to-image conversion and symmetry constraint.

Table 2. Quantitative comparison of EMD and F-Score on three categories. EMD values are multiplied by 10^{-2}.

Method	EMD↓				F-Score↑			
	Chair	Car	Airplane	Avg	Chair	Car	Airplane	Avg
Point-E[43]	2.94	3.58	1.73	2.75	0.35	0.19	0.53	0.36
RGB2Point[30]	2.20	0.85	0.45	1.17	0.53	0.91	**0.99**	0.81
Ours	**1.65**	**0.27**	**0.44**	**0.79**	**0.95**	**0.99**	**0.99**	**0.98**
w/o Sketch-to-Image	1.75	0.77	0.52	1.01	0.87	0.90	0.98	0.92
w/o Symmetry	1.77	0.34	0.45	0.85	0.94	0.98	**0.99**	0.97

3.5. Comparison with Diffusion-based Methods

To address the concern that non-diffusion methods might be inferior to diffusion-based approaches, we compare our method with two representative diffusion-based approaches: SDFusion [47] and LAS-Diffusion [18]. Both methods are based on mesh generation. As shown in Fig. 4, our method demonstrates superior visual quality compared to these diffusion-based methods. The left half of Fig. 4 shows results on synthetic sketches, while the right half displays results on hand-drawn sketches.

Table 3 presents a comprehensive comparison in terms of computational efficiency and model complexity. Our method significantly outperforms the diffusion-based approaches in both inference time and parameter count. This comparison demonstrates that our non-diffusion approach not only produces superior visual results but also offers substantial advantages in computational efficiency and resource utilization.

Table 3. Computation complexity analysis.

Method	Inference Time	Params
SDFusion[47]	7.17s	1126.34M
LAS-Diffusion[18]	25.99s	699.94M
Ours	**2.37s**	**324.69M**

4. CONCLUSION

In this study, we propose a novel two-stage method for sketch-to-3D shape generation that introduces images as intermediate semantic bridges and employs symmetry-aware geometric reconstruction.

Our method shows competitive results compared to state-of-the-art methods on ShapeNet-related datasets. Experiments verify our method's superiority in reconstruction accuracy and structural integrity. This research provides a novel technical pathway for 3D modeling based on non-expert user inputs. Future work will extend our approach to better handle asymmetric objects, broadening applicability to more diverse and complex shapes.

5. REFERENCES

[1] Xian-Feng Han, Hamid Laga, and Mohammed Bennamoun, "Image-based 3d object reconstruction: State-of-the-art and trends in the deep learning era," *IEEE transactions on pattern analysis and machine intelligence*, vol. 43, no. 5, pp. 1578–1604, 2019.

[2] Rohan Agarwal, Wei Zhou, Xiaofeng Wu, and Yuhan Li, "Efficient 3d object reconstruction using visual transformers," *arXiv preprint arXiv:2302.08474*, 2023.

[3] Shijie Zhang, Boyan Jiang, Keke He, Junwei Zhu, Ying Tai, Chengjie Wang, Yinda Zhang, and Yanwei Fu, "T-pixel2mesh: Combining global and local transformer for 3d mesh generation from a single image," *arXiv preprint arXiv:2403.13663*, 2024.

[4] Shentong Mo, Enze Xie, Ruihang Chu, Lanqing Hong, Matthias Niessner, and Zhenguo Li, "Dit-3d: Exploring plain diffusion transformers for 3d shape generation," *Advances in neural information processing systems*, vol. 36, pp. 67960–67971, 2023.

[5] Yuhan Li, Yishun Dou, Xuanhong Chen, Bingbing Ni, Yilin Sun, Yutian Liu, and Fuzhen Wang, "Generalized deep 3d shape prior via part-discretized diffusion process," in *Proceedings of the IEEE/CVF Conference on Computer Vision and Pattern Recognition*, 2023, pp. 16784–16794.

[6] Manyi Li and Hao Zhang, "D2im-net: Learning detail disentangled implicit fields from single images," in *Proceedings of the IEEE/CVF Conference on Computer Vision and Pattern Recognition*, 2021, pp. 10246–10255.

[7] Muheng Li, Yueqi Duan, Jie Zhou, and Jiwen Lu, "Diffusion-sdf: Text-to-shape via voxelized diffusion," in *Proceedings of the IEEE/CVF conference on computer vision and pattern recognition*, 2023, pp. 12642–12651.

[8] Biao Zhang, Jiapeng Tang, Matthias Niessner, and Peter Wonka, "3dshape2vecset: A 3d shape representation for neural fields and generative diffusion models," *ACM Transactions On Graphics (TOG)*, vol. 42, no. 4, pp. 1–16, 2023.

[9] Yushi Lan, Fangzhou Hong, Shuai Yang, Shangchen Zhou, Xuyi Meng, Bo Dai, Xingang Pan, and Chen Change Loy, "Ln3diff: Scalable latent neural fields diffusion for speedy 3d generation," in *European Conference on Computer Vision*. Springer, 2024, pp. 112–130.

[10] Jaehyeok Shim, Changwoo Kang, and Kyungdon Joo, "Diffusion-based signed distance fields for 3d shape generation," in *Proceedings of the IEEE/CVF conference on computer vision and pattern recognition*, 2023, pp. 20887–20897.

[11] Ruikai Cui, Weizhe Liu, Weixuan Sun, Senbo Wang, Taizhang Shang, Yang Li, Xibin Song, Han Yan, Zhennan Wu, Shenzhou Chen, et al., "Neusdfusion: A spatial-aware generative model for 3d shape completion, reconstruction, and generation," in *European Conference on Computer Vision*. Springer, 2024, pp. 1–18.

[12] Maxim Tatarchenko, Alexey Dosovitskiy, and Thomas Brox, "Octree generating networks: Efficient convolutional architectures for high-resolution 3d outputs," in *Proceedings of the IEEE international conference on computer vision*, 2017, pp. 2088–2096.

[13] Roman Klokov, Edmond Boyer, and Jakob Verbeek, "Discrete point flow networks for efficient point cloud generation," in *European Conference on Computer Vision*. Springer, 2020, pp. 694–710.

[14] Linqi Zhou, Yilun Du, and Jiajun Wu, "3d shape generation and completion through point-voxel diffusion," in *Proceedings of the IEEE/CVF international conference on computer vision*, 2021, pp. 5826–5835.

[15] Yue Zhong, Yonggang Qi, Yulia Gryaditskaya, Honggang Zhang, and Yi-Zhe Song, "Towards practical sketch-based 3d shape generation: The role of professional sketches," *IEEE Transactions on Circuits and Systems for Video Technology*, vol. 31, no. 9, pp. 3518–3528, 2020.

[16] Chenjian Gao, Qian Yu, Lu Sheng, Yi-Zhe Song, and Dong Xu, "Sketchsampler: Sketch-based 3d reconstruction via view-dependent depth sampling," in *European Conference on Computer Vision*. Springer, 2022, pp. 464–479.

[17] Song-Hai Zhang, Yuan-Chen Guo, and Qing-Wen Gu, "Sketch2model: View-aware 3d modeling from single free-hand sketches," in *Proceedings of the IEEE/CVF Conference on Computer Vision and Pattern Recognition*, 2021, pp. 6012–6021.

[18] Xin-Yang Zheng, Hao Pan, Peng-Shuai Wang, Xin Tong, Yang Liu, and Heung-Yeung Shum, "Locally attentional sdf diffusion for controllable 3d shape generation," *ACM Transactions on Graphics (ToG)*, vol. 42, no. 4, pp. 1–13, 2023.

[19] Jie Zhou, Zhongjin Luo, Qian Yu, Xiaoguang Han, and Hongbo Fu, "Ga-sketching: Shape modeling from multi-view sketching with geometry-aligned deep implicit functions," in *Computer Graphics Forum*. Wiley Online Library, 2023, vol. 42, p. e14948.

[20] Minglin Chen, Weihao Yuan, Yukun Wang, Zhe Sheng, Yisheng He, Zilong Dong, Liefeng Bo, and Yulan Guo, "Sketch2nerf: multi-view sketch-guided text-to-3d generation," *arXiv preprint arXiv:2401.14257*, 2024.

[21] Haiyang Ying and Matthias Zwicker, "Sketchsplat: 3d edge reconstruction via differentiable multi-view sketch splatting," *arXiv preprint arXiv:2503.14786*, 2025.

[22] Aditya Sanghi, Pradeep Kumar Jayaraman, Arianna Rampini, Joseph Lambourne, Hooman Shayani, Evan Atherton, and Saeid Asgari Taghanaki, "Sketch-a-shape: Zero-shot sketch-to-3d shape generation," *arXiv preprint arXiv:2307.03869*, 2023.

[23] Dan Wang, Xinrui Cui, Xun Chen, Zhengxia Zou, Tianyang Shi, Septimiu Salcudean, Z Jane Wang, and Rabab Ward, "Multi-view 3d reconstruction with transformers," in *Proceedings of the IEEE/CVF international conference on computer vision*, 2021, pp. 5722–5731.

[24] Yue Shan, Jun Xiao, Lupeng Liu, Yunbiao Wang, Dongbo Yu, and Wenniu Zhang, "A coarse-to-fine transformer-based network for 3d reconstruction from non-overlapping multi-view images," *Remote Sensing*, vol. 16, no. 5, pp. 901, 2024.

[25] Titas Anciukevičius, Zexiang Xu, Matthew Fisher, Paul Henderson, Hakan Bilen, Niloy J Mitra, and Paul Guerrero, "Renderdiffusion: Image diffusion for 3d reconstruction, inpainting and generation," in *Proceedings of the IEEE/CVF conference on computer vision and pattern recognition*, 2023, pp. 12608–12618.

[26] Seunggwan Lee, Hwanhee Jung, Byoungsoo Koh, Qixing Huang, Sangho Yoon, and Sangpil Kim, "Pasta: Part-aware sketch-to-3d shape generation with text-aligned prior," *arXiv preprint arXiv:2503.12834*, 2025.

[27] Hail Song, Wonsik Shin, Naeun Lee, Soomin Chung, Nojun Kwak, and Woontack Woo, "S3d: Sketch-driven 3d model generation," *arXiv preprint arXiv:2505.04185*, 2025.

[28] Feng-Lin Liu, Hongbo Fu, Yu-Kun Lai, and Lin Gao, "Sketchdream: Sketch-based text-to-3d generation and editing," *ACM Transactions on Graphics (TOG)*, vol. 43, no. 4, pp. 1–13, 2024.

[29] Fangneng Zhan, Yingchen Yu, Rongliang Wu, Jiahui Zhang, Shijian Lu, and Changgong Zhang, "Marginal contrastive correspondence for guided image generation," in *Proceedings of the IEEE/CVF conference on computer vision and pattern recognition*, 2022, pp. 10663–10672.

[30] Jae Joong Lee and Bedrich Benes, "Rgb2point: 3d point cloud generation from single rgb images," *arXiv preprint arXiv:2407.14979*, 2024.

[31] Xingyi Li, Chaoyi Hong, Yiran Wang, Zhiguo Cao, Ke Xian, and Guosheng Lin, "Symmnerf: Learning to explore symmetry prior for single-view view synthesis," in *Proceedings of the Asian conference on computer vision*, 2022, pp. 1726–1742.

[32] Qiangeng Xu, Weiyue Wang, Duygu Ceylan, Radomir Mech, and Ulrich Neumann, "Disn: Deep implicit surface network for high-quality single-view 3d reconstruction," *Advances in neural information processing systems*, vol. 32, 2019.

[33] Abhishek Kar, Christian Häne, and Jitendra Malik, "Learning a multi-view stereo machine," *Advances in neural information processing systems*, vol. 30, 2017.

[34] Angel X Chang, Thomas Funkhouser, Leonidas Guibas, Pat Hanrahan, Qixing Huang, Zimo Li, Silvio Savarese, Manolis Savva, Shuran Song, Hao Su, et al., "Shapenet: An information-rich 3d model repository," *arXiv preprint arXiv:1512.03012*, 2015.

[35] Pan Zhang, Bo Zhang, Dong Chen, Lu Yuan, and Fang Wen, "Cross-domain correspondence learning for exemplar-based image translation," in *Proceedings of the IEEE/CVF conference on computer vision and pattern recognition*, 2020, pp. 5143–5153.

[36] Fangneng Zhan, Yingchen Yu, Rongliang Wu, Jiahui Zhang, Shijian Lu, and Changgong Zhang, "Marginal contrastive correspondence for guided image generation," in *Proceedings of the IEEE/CVF conference on computer vision and pattern recognition*, 2022, pp. 10663–10672.

[37] Baran Ozaydin, Tong Zhang, Sabine Susstrunk, and Mathieu Salzmann, "Dsi2i: Dense style for unpaired exemplar-based image-to-image translation," *Transactions on Machine Learning Research*, 2024.

[38] Diederik Kinga, Jimmy Ba Adam, et al., "A method for stochastic optimization," in *International conference on learning representations (ICLR)*. California;, 2015, vol. 5.

[39] Takeru Miyato, Toshiki Kataoka, Masanori Koyama, and Yuichi Yoshida, "Spectral normalization for generative adversarial networks," *arXiv preprint arXiv:1802.05957*, 2018.

[40] Tianrun Chen, Runlong Cao, Zejian Li, Ying Zang, and Lingyun Sun, "Deep3dsketch-im: rapid high-fidelity ai 3d model generation by single freehand sketches," *Frontiers of Information Technology & Electronic Engineering*, vol. 25, no. 1, pp. 149–159, 2024.

[41] Tianrun Chen, Chenglong Fu, Lanyun Zhu, Papa Mao, Jia Zhang, Ying Zang, and Lingyun Sun, "Deep3dsketch: 3d modeling from free-hand sketches with view-and structural-aware adversarial training," *arXiv preprint arXiv:2312.04435*, 2023.

[42] Benoit Guillard, Edoardo Remelli, Pierre Yvernay, and Pascal Fua, "Sketch2mesh: Reconstructing and editing 3d shapes from sketches," in *Proceedings of the IEEE/CVF International Conference on Computer Vision*, 2021, pp. 13023–13032.

[43] Alex Nichol, Heewoo Jun, Prafulla Dhariwal, Pamela Mishkin, and Mark Chen, "Point-e: A system for generating 3d point clouds from complex prompts," *arXiv preprint arXiv:2212.08751*, 2022.

[44] Christopher B Choy, Danfei Xu, JunYoung Gwak, Kevin Chen, and Silvio Savarese, "3d-r2n2: A unified approach for single and multi-view 3d object reconstruction," in *Computer vision–ECCV 2016: 14th European conference, amsterdam, the netherlands, October 11-14, 2016, proceedings, part VIII 14*. Springer, 2016, pp. 628–644.

[45] Andrew Brock, Jeff Donahue, and Karen Simonyan, "Large scale gan training for high fidelity natural image synthesis," *arXiv preprint arXiv:1809.11096*, 2018.

[46] Alexey Dosovitskiy, Lucas Beyer, Alexander Kolesnikov, Dirk Weissenborn, Xiaohua Zhai, Thomas Unterthiner, Mostafa Dehghani, Matthias Minderer, Georg Heigold, Sylvain Gelly, et al., "An image is worth 16x16 words: Transformers for image recognition at scale," *arXiv preprint arXiv:2010.11929*, 2020.

[47] Yen-Chi Cheng, Hsin-Ying Lee, Sergey Tulyakov, Alexander G Schwing, and Liang-Yan Gui, "Sdfusion: Multimodal 3d shape completion, reconstruction, and generation," in *Proceedings of the IEEE/CVF conference on computer vision and pattern recognition*, 2023, pp. 4456–4465.